Integrated Approach for Modeling the Emission Fluorescence of 4-(*N*,*N*-Dimethylamino)benzonitrile in Polar Environments

Silvia Carlotto,[†] Antonino Polimeno,*[,†] Camilla Ferrante,[†] Caterina Benzi,[‡] and Vincenzo Barone[‡]

Dipartimento di Scienze Chimiche, Università degli Studi di Padova, Via Marzolo 1-35131 Padova, Italy, and Dipartimento di Chimica, Università di Napoli "Federico II", Complesso Universitario di Monte Sant'Angelo Via Cintia, I-80126 Napoli, Italy

Received: August 20, 2007; Revised Manuscript Received: February 23, 2008

A stochastic model for the interpretation of the emission fluorescence of 4-(*N*,*N*-dimethylamino)benzonitrile (DMABN) is discussed. We proceed by reviewing the stochastic modeling approach (Polimeno, A.; Barbon, A.; Nordio, P. L.; Rettig, W. *J. Phys. Chem.* 1994, *98*, 12158), in which internal degrees of freedom are coupled with an effective solvent relaxation variable. Potential energy surfaces are obtained using a reliable but computationally cost-effective quantum mechanical (QM) approach, and estimates of dissipative parameters are calculated on the basis of direct hydrodynamic arguments. Emission fluorescence is estimated by solving numerically a diffusion/sink/source equation for the stationary population of excited state and compared to emission fluorescence of DMABN measured experimentally.

I. Introduction

Since the seminal studies[1] of the dual fluorescent behavior of 4-(*N*,*N*-dimethylamino)benzonitrile (DMABN) in polar solvents, this molecule has been the subject of several experimental[2–4] and theoretical studies.[5–9] The emission spectrum of DMABN presents two fluorescence bands strongly dependent on the solvent polarity and temperature. In low-polarity solvents, only a band is usually observed (locally excited, LE) at high frequency, whereas, in highly polar solvents, a second band is present at low frequency, usually interpreted as resulting from a twisted intramolecular charge transfer state (TICT) phenomenon. Intermediate behaviors, when both LE and TICT bands are present, are observed in medium-polarity solvents.

This evidence can be explained qualitatively by the well-known Grabowski model,[5,10] which links the charge transfer reaction (LE−TICT) to a twisting motion and orbital decoupling of the phenyl acceptor ring from the electron donor group. In short, DMABN can be thought to possess a double-minimum potential in its excited state. In the ground state, the donor and acceptor moieties are planar; the molecule in its first excited state can twist the dimethylamino group from a planar to perpendicular conformation with respect to the phenyl ring. The twisting motion is accompanied by a charge transfer from donor to acceptor in the excited state. The dual fluorescence in DMABN arises from the two lowest singlet excited states, because each has a different geometry at which it attains a minimum. The LE state is the lowest excited singlet state of the DMABN and is the origin of the LE band in the fluorescence spectrum, whereas the TICT state is the second excited singlet state and is the cause of the TICT band in the spectrum of DMABN: it has a strong minimum with a 90° twisted amino group conformation and an exceedingly high dipole moment. These two states have an intersection region with strong vibronic coupling, which allows for transitions between LE and TICT. A quantitative description of the excited-state dynamics can be obtained by considering the angle between the amino group and the aromatic plane as a relevant internal degree of freedom and adopting a stochastic description for its time evolution[9–15] to describe the charge transfer process of the excited state that accompanies torsional motion. The internal coordinate is coupled to a solvent polarization coordinate defined as the stochastic reaction field in an Onsager cavity.[15] The time evolution equation for the excited-state population is determined by a Smoluchowski operator modified by inclusion of sink and source terms. Basic ingredients of the model are (i) the total energy of the solute−solvent system in the two excited states and in the ground state, which is given as the sum of the potential energy of the isolated molecule and a solvent correction; and (ii) the diffusion coefficients for the internal motion and for the solvent relaxation.

In this work, we are interested in defining a coarse-grained description of solvation dynamics to understand the main effects of polar media on the observed emission fluorescence of DMABN as a prototype model that will also be employed for more complex systems[16,17] that are particularly interesting for their metal-binding properties, such as fluorescent ionophore DMABN−cyclam,[18–20] 4-(1-aza-4,7,10-trioxacyclododecyl)benzonitrile (DMABN−crown4), and 4-(1-aza-4,7,10,13-tetraoxacyclododecyl)benzonitrile (DMABN−crown5).[21] We seek a relatively simple interpretation based on macroscopic solvent properties (dielectric constants and viscosity), keeping at a minimum the number of adjustable parameters. To do so, we shall consider a stochastic diffusive description of the molecule internal dynamics, an explicit evaluation of dissipative properties (diffusion tensor) from a simplified hydrodynamic description of the solute molecule, and a simple characterization of solvent variables. The methodology is based on a three-step procedure; namely, (1) the definition of potential energy surfaces for the ground state and the two lowest-energy excited states of the solute molecules in vacuo, (2) coupled with a description for the roto-translational and conformational dynamics in the presence of a (3) stochastic polarization coordinates representing the solvent relaxation. We intend to combine computational cost

* Corresponding author. Phone: ++390498275146. Fax: ++390498275239. E-mail: antonino.polimeno@unipd.it.
[†] Università degli Studi di Padova.
[‡] Università di Napoli "Federico II".

10.1021/jp076676z CCC: $40.75
Published on Web 06/14/2008

effectiveness with semiquantitative predictive capability. To do so, we test in this work the overall methodology for the DMABN case, building on previous work.[15]

The Article is organized as follows: In section II, we define the basic model for DMABN, describing the molecular dynamic behavior, including a simplified description of internal dynamics in terms of a single conformational coordinate. Evaluation of potential energy surfaces (PES) is carried out using advanced quantum mechanical (QM) approaches. Diffusive parameters are obtained from standard hydrodynamic arguments. Roto-translation invariance and an approximate solute−solvent coupling potential are used to simplify the dynamic description. In section III, the model is discussed, and approximate solution methods are presented. Examples of simulated emission spectra in various solvents are provided to test the model versatility, and they are compared with available literature data on solvatochromic effects of static emission of DMABN in section IV.

II. Methods

We review here briefly a phenomenological approach to the calculation of the emission fluorescence signal[12–15] in DMABN. The (time-dependent) emission fluorescence signal $I(\omega, t)$ for a generic molecular system can be in general written as an integral over excited-state phase space variables

$$I(\omega,t) \propto \int \mathrm{d}Q \sum_n k^{\mathrm{rad}}_{n\to \mathrm{g}}(Q)\, g_n[\omega - \Delta\omega_n(Q)]\, P_n(Q,t) \quad (1)$$

Here, we shall denote with collective index Q the coordinates (in a broad sense, to be specified later as the chosen variables describing the instantaneous solute + solvent configuration) for a given configuration. The sum runs over excited states $n = 1,..., N$. The quantity $\Delta\omega_n(z)$ is the difference between state n and the ground state, g, $\hbar\Delta\omega_n(Q) = E_n(Q) - E_g(Q)$, $k^{\mathrm{rad}}_{n\to \mathrm{g}}(Q)$ is the radiative emission factor for state n to ground state, and $g_n(\omega)$ is an intrinsic line shape. The excited-state populations, $P_n(Q, t)$ are described by a time evolution equation that is based on a stochastic operator, $\hat{\Gamma}_n$, describing internal relaxation processes affecting the excited state; source terms $S_n(Q, t)$ for the creation of the excited-state population; and kinetic terms accounting for radiative and nonradiative decay to ground state and coupling among excited states

$$\frac{\partial}{\partial t}P_n(Q,t) = -\hat{\Gamma}_n\, P_n(Q,t) - \sum_{n'} k_{nn'}(Q)\, P_{n'}(Q,t) + S_n(Q,t) \quad (2)$$

with suitable initial conditions; for example, simply $P_n(Q, t) = 0$. By modeling $\hat{\Gamma}_n$, $k_{nn'}(Q)$, and $S_n(Q, t)$, the dynamic or static emission can be reproduced. The stationary emission spectrum is obtained in particular as

$$I(\omega) \propto \int \mathrm{d}Q \sum_n k^{\mathrm{rad}}_{n\to \mathrm{g}}(Q)\, g_n[\omega - \Delta\omega_n(Q)]\, P_{\mathrm{st},n}(Q) \quad (3)$$

where the stationary population for all excited states is obtained as

$$\hat{\Gamma}_n\, P_{\mathrm{st},n}(Q) + \sum_{n'} k_{nn'}(Q)\, P_{\mathrm{st},n'}(Q) = S_n(Q) \quad (4)$$

where $S_n(Q)$ is the stationary source function. To summarize, the dynamic or static fluorescence emission is in principle obtainable after defining a suitable pump and kinetic term; both generic functions of the system variables (including internal solute conformational degrees of freedom plus solvent configuration coordinates); radiative emission factors $k^{\mathrm{rad}}_n(Q)$; intrinsic shape functions $g_n(\omega)$; and, above all, time evolution operators $\hat{\Gamma}_n$, which are defined as a stochastic operator for the time evolution along the Q coordinates in the nth excited state and are fully specified with respect to the potential energy surfaces of the excited state.

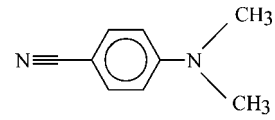

(DMABN)

Figure 1. Structures of 4-(*N*,*N*-dimethylamino)benzonitrile (DMABN).

A. The Model. We start by providing explicit forms for eqs 1–4 for the case of DMABN. We consider two diabatic states, n = A, B. The molecular structure is summarized in Figure 1. An internal coordinate, φ, describing the donor/acceptor's relative orientation is introduced as the main degree of freedom describing internal conformational dynamics. The phase space variables are described in principle as $Q = (\Omega, \varphi, \mathbf{X})$; that is, orientational coordinates Ω for the position of the molecular frame (MF) in space, plus internal coordinate φ and fluctuating solvent polarization vector $\mathbf{X}$, with components naturally defined in the laboratory (inertial) frame (LF).[12] We write the PES for each state in the form

$$E_n(Q) = \varepsilon_n(\Omega,\varphi) - \frac{F_\infty}{2}\mu_n{}^2(\varphi) - \boldsymbol{\mu}_n(\Omega,\varphi)\cdot\mathbf{X} + \frac{1}{2F_{\mathrm{or}}}X^2 \quad (5)$$

$\varepsilon_n(\Omega, \varphi)$ is the in vacuo energy of the nth excited state, depending upon the internal geometry; $\boldsymbol{\mu}_n(\Omega, \varphi)$ is the electric dipole moment vector of the molecule in the nth excited state, with components in LF; the term $(F_\infty/2)\mu_n{}^2(\varphi)$ represents the solvation energy due to electric polarization; and $\boldsymbol{\mu}_n(\Omega, \varphi)\cdot\mathbf{X}$ derives from solute−solvent interaction due to orientational polarization. The last term, $(1/2F_{\mathrm{or}})X^2$, accounts for the solvent coordinate fluctuations. Onsager theory in its simplest form (solute as a spherical cavity of volume V) gives us explicit estimates of F_0, F_∞, and $F_{\mathrm{or}} = F_0 - F_\infty$:

$$F_{0,\infty} = \frac{1}{4\pi V\varepsilon_{\mathrm{vacuo}}}\,\frac{2(\varepsilon_{0,\infty}-1)}{2\varepsilon_{0,\infty}+1} \quad (6)$$

where $\varepsilon_{\mathrm{vacuo}}$ is the dielectric permittivity in vacuo.[15] The time evolution operator, $\hat{\Gamma}_n$, describing the molecule dynamics, is defined as the diffusive operator

$$\hat{\Gamma}_n = -\left(\hat{\mathbf{M}}\frac{\partial}{\partial\varphi}\right)^{\mathrm{tr}}\cdot\mathbf{D}_n\cdot P_{\mathrm{eq},n}(Q)\begin{pmatrix}\hat{\mathbf{M}}\\ \frac{\partial}{\partial\varphi}\end{pmatrix}P_{\mathrm{eq},n}{}^{-1}(Q) - \left(\frac{\partial}{\partial\mathbf{X}}\right)^{\mathrm{tr}}\cdot\mathbf{D}_{\mathrm{S}}\cdot P_{\mathrm{eq},n}(Q)\left(\frac{\partial}{\partial\mathbf{X}}\right)P_{\mathrm{eq},n}{}^{-1}(Q) \quad (7)$$

where n = A, B and where the solute gradient operator is $(\hat{\mathbf{M}}(\partial/\partial\varphi))$ and depends upon the rotational infinitesimal operator $\hat{\mathbf{M}}$[22] and internal rotation $\partial/\partial\varphi$. The function $P_{\mathrm{eq},n}$ is defined as the equilibrium (Boltzmann) distribution with respect to the total energy, E_n. Diffusion tensors $\mathbf{D}_n$ and $\mathbf{D}_{\mathrm{S}}$ are defined for the solute and solvent motion. We can write the general expression for $\mathbf{D}_n$

$$\mathbf{D}_n = \begin{pmatrix}\mathbf{D}_{\mathrm{R},n} & \mathbf{D}_{\mathrm{RI},n}\\ \mathbf{D}^{\mathrm{tr}}_{\mathrm{RI},n} & D_{\mathrm{I},n}\end{pmatrix} \quad (8)$$

where blocks $\mathbf{D}_{\mathrm{R},n}$, $\mathbf{D}_{\mathrm{RI},n}$, and $D_{\mathrm{I},n}$ are related to purely rotational, rotational−conformational, and purely conformational diffusive

motion, respectively, and they can be estimated using hydrodynamic arguments. Solvent polarization diffusion is described by diffusion tensor $\mathbf{D}_S$, which can be related to solvent relaxation times, as specified in the following paragraphs.

In principle, eqs 7 and 8 allow the description of the joint relaxation of a molecule in state n, rotating in space and subject to internal conformational dynamics, coupled to a solvent polarization vectorial coordinate. No rotational invariance has been invoked yet, and thus, a physical environment that is characterized by rotational anisotropy, such as nematic or smectic liquid crystals, can be described. In the case of polar isotropic fluids, one can (1) average out the dependence upon rotational coordinates Ω; (2) refer the solvent coordinate vector the molecular frame MF (which is supposed to be essentially the same in all states) chosen to have one axis along internal dipole $\boldsymbol{\mu}_n = \mu_n(\varphi)\mathbf{u}_n$; (3) assume that $x = \mathbf{X}\cdot\mathbf{u}_n$; that is, the component of solvent polarization along the dipole is the major source of coupling in eq 8 and neglect other components; (4) assume that no significant coupling exists between internal and conformational degrees of freedom; that is, neglect nondiagonal blocks in eq 8 and residual dependence of diagonal blocks upon internal coordinate φ; in addition, to a first approximation, differences in shape in states are neglected, leading to a single dissipative parameter $D_{I,n} \approx D_I$ for internal rotation; and finally (5) assume a scalar approximation for tensor $\mathbf{D}_S = D_S\mathbf{1}$. Assumptions 1 and 2 are exact statements consequent from the assumption of rotational isotropy; 3, 4, and 5 are approximations based on the idea that static and dynamic properties are mainly represented by coordinates $Q = (\varphi, x)$. The simplified time evolution operator is now given by

$$\hat{\Gamma}_n = -D_I \frac{\partial}{\partial\varphi} P_{eq,n}(\varphi,x) \frac{\partial}{\partial\varphi} P_{eq,n}{}^{-1}(\varphi,x) - D_S \frac{\partial}{\partial x} P_{eq,n}(\varphi,x) \frac{\partial}{\partial x} P_{eq,n}{}^{-1}(\varphi,x) \quad (9)$$

where n = A, B. The kinetic terms in eq 3 need yet to be defined. Assuming that both radiative and nonradiative processes are taken into account, we can write $k_{AA} = k^{nr}_{A\to B} + k^{nr}_{A\to g} + k^{rad}_{A\to g}$, $k_{BB} = k^{nr}_{B\to A} + k^{nr}_{B\to g} + k^{rad}_{B\to g}$, $k_{AB} = -k^{nr}_{B\to A}$, and $k_{BA} = -k^{nr}_{A\to B}$, where $k^{nr}_{A\to g}$ and $k^{rad}_{A\to g}$ are kinetic coefficients (in general depending upon φ) for nonradiative and radiative decay to ground state from state A, $k^{nr}_{A\to B}$ is the kinetic coefficient for (assumed nonradiative) transition A $\rightarrow$ B, and so on. To summarize: for the case of fluorescence emission of DMABN, with two diabatic states A and B, both emitting to the g state, with one conformational degree of freedom φ, in the presence of coupling with one effective solvent coordinate x in a polar aprotic isotropic solvent, the following basic functions and model parameters are needed: dielectric constants $\varepsilon_{0,\infty}$ and estimate of the molecular volume V to evaluate $F_{0,\infty}$ parameters; in vacuo PES $\varepsilon_n(\varphi)$ and electric dipole moment $\boldsymbol{\mu}_n(\varphi)$ obtained from QM calculations for A, B, and g states; relaxation coefficients D_I (for internal dynamics) and D_S (solvent relaxation), which can be related to molecular geometry and solvent macroscopic properties; and kinetic coefficients $k^{nr}_{A\to g}$, $k^{nr}_{B\to g}$, $k^{nr}_{A\to B}$, $k^{nr}_{B\to A}$, $k^{rad}_{A\to g}$, and $k^{rad}_{B\to g}$. Finally, to evaluate the stationary emission fluorescence according to eq 3, we need to specify functions $S_n(\varphi, x)$ and $g_n(\omega)$.

B. Parameters. Several theoretical investigations have been published in recent years for the interpretation of the fluorescence properties of DMABN. The reduced size of the molecule allows an investigation by ab initio methods,[23,24] but semiempirical methods are still applied.[25,26] Many theoretical investigations have been conducted for the ground state, but few calculations have been described for the excited states that include the optimization of excited-state geometries.[27] The single-reference configuration interactions with single excitations (CIS) is frequently used,[7,28] but sometimes the order of the energies of the excited states in not reproduced correctly.[29] The complete active space self-consistent field (CASSCF) method is a good approach to consider the nondynamic electron correlation effects.[30,31] CIS and CASSCF methods often give poor geometries for excited states because they do not include the dynamical electron correlations,[32] whereas the complete active space second-order perturbation theory (CASPT2) includes the dynamic correlation effects that are important for obtaining a quantitative accordance with the energies. Density functional theory (DFT)-based methods have proved to be a significant progress for the evaluation of excited-state properties with the time-dependent DFT (TDDFT),[33] a combination of DFT with a single or multireference[34] configuration interaction. TDDFT gives more accurate geometries and excitation energies than those of low-level ab initio theories with a low computational cost equivalent to that of CIS. Recently, it was suggested that the poor behavior of charge transfer excitations by TDDFT are solved by applying the long-range correction to the TDDFT scheme.[32]

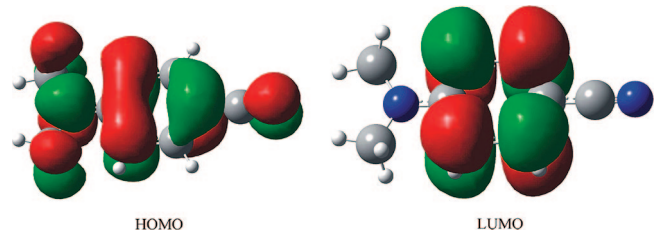

Figure 2. Schematic drawings of selected molecular orbitals (HOMO and LUMO) for DMABN at ground-state geometry.

We start by considering the PES and electric dipole moment for DMABN. Among computational methods apt to describe excited states, time-dependent density functional theory (TDDFT; for a survey of ground-state DFT, see, for example, ref 23) is gaining more and more attention in the study of medium- and large-sized molecules, thanks to its favorable balance between accuracy and computational demand. The recent implementation of TDDFT analytical gradients[35] both in vacuo and in solution allows for the determination of excited-state stationary points and properties (such as multipole moments); moreover, harmonic frequencies can be calculated by numerical differentiation of the analytic gradients, and the subsequent vibrational analysis is providing encouraging results.

The use of TDDFT has been limited by some deficiencies in properly describing excited states involving charge separation or with contributions from double excitations.[36–39] Recently, some interesting attempts to overcome these limitations have been proposed.[38–44] On the other hand, for electronic transitions which involve only partial intramolecular charge transfer (TICT), the underestimation of excitation energies by TDDFT, due to spurious self-interaction, may be controlled by the use of hybrid functionals. This is the case for DMABN, in which the highest occupied molecular orbital (HOMO) and the lowest unoccupied molecular orbital (LUMO) involved in the TICT transition partially overlap (Figure 2).

Here, TDDFT results for absorption energies for the two lowest states of DMABN are presented at the geometry of the ground-state minimum (C_{2v} symmetry) optimized at the PBE0/6-31G(d) level of theory. The same hybrid functional[45] has also been employed for TDDFT calculations, because it is known

TABLE 1: Absorption Energies (eV) for DMABN in Vacuo at the TDDFT Level Employing the PBE0 Functional and Different Basis Sets[a]

	LE	TICT
experimental (ref 51)	4.25 (0.031) ± 0.1	4.56 (0.680) ± 0.1
TDDFT/6-31G(d)	4.68 (0.0276)	4.85 (0.5546)
TDDFT/6-311+G(d,p)	4.49 (0.0338)	4.72 (0.5529)
TDDFT/aug-cc-pVTZ	4.45 (0.0319)	4.71 (0.5489)
main contr.	HOMO → LUMO + 1	HOMO → LUMO

[a] Oscillatory strength is given in parentheses. MO main contributions for each transition are also shown.

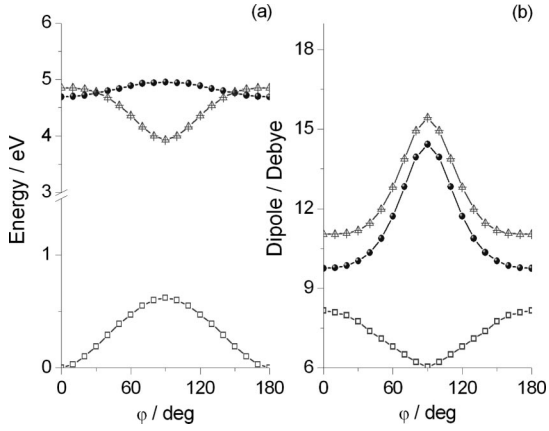

Figure 3. (a) Ground (square) and low-lying singlet excited state (A in circle and B in triangle) potential energy surfaces of DMABN in vacuo as a function of the torsional angle (in degrees). The energy (expressed in eV) is relative to the minimum of the ground state. (b) Ground and low-lying singlet excited state dipole moment curves of DMABN in vacuo as a function of the torsional angle (in degrees).

that the hybridization with Hartree−Fock exchange partly overcomes the self-interaction error. Despite the absence of adjustable parameters, when employed in TDDFT calculations, PBE0 (TD-PBE0) has already provided excitation spectra in very good agreement with the available experimental results.[46,47] Different basis sets have been tested: first, we used the Pople family of basis sets 6-31G,[48] with different contraction schemes and the addition of polarization[49] and diffuse functions,[50] and then the aug-cc-pVDZ basis set. Results are collected in Table 1 and are compared with experimental data.[51]

Gas-phase calculations for the CT state provide differences from experimental values (ΔE) ranging between 0.29 (6-31G(d) basis set) and 0.14 eV (aug-cc-pVDZ). TDDFT calculations, taken from the literature,[33] performed using the B3LYP functional and TZVPP basis sets provided $\Delta E = 0.11$ eV.

All TDDFT excitation energies are close to their counterparts issuing from post-HF computations, such as multireference perturbation configuration interaction (CIPSI,[7] $\Delta E = 0.22$ eV), CASPT2/ANO(DZ)[52] ($\Delta E = -0.18$ eV), and STEOM-CCSD/cc-pVTZ[53] ($\Delta E = 0.14$ eV). Moreover, the energy differences between the LE and CT states is also well reproduced by TDDFT. All calculations have been performed by exploiting a development version of the Gaussian code.[54]

As shown in Figure 3a, the ground state presents a valley along the torsional angle. The minimum is found at the full planar geometry. We consider the energy of this minimum as the energy reference. The g state presents a maximum at 90°, and the energetic barrier is 0.6 eV, in accordance with literature data.[7] During the evaluation of the energy, the geometry has been kept frozen to that optimized for the ground state for every point and for both excited states. The only changing parameter is the torsional angle between the donor and the acceptor, which has been varied from 0 to 180° in steps of 10°. The first excited state, the LE state called A in this work, shows a minimum energy as in the g state at the full planar geometry (4.68 eV). The TICT state (B state) presents a flat region (4.85 eV) around the planar conformation until the intersection region near 45°. From this point, the energy of this state decreases until a minimum at 90° (3.95 eV). Figure 3b describes the trend of the dipole moment for the ground state and for the two lowest-energy excited states as a function of the torsional angle. The ground-state dipole moment (in green) decreases with the increase of the torsional angle with a gap of −2.12 D from 0 to 90°. As for the energy calculations, the torsional angle is varied with a step of 10° in the same range. The dipole moment of the TICT state increases with the torsional angle until a maximum at 90° with a gap of 15.5 D in vacuo.

Next, we consider the diffusion coefficient associated with internal rotation, $D_{I,n}(\varphi) \approx D_I = 1/\tau_I$. Following the hydrodynamic approach[55] summarized in the Appendix, we consider the molecule as a collection of identical spheres of radius R linked by rigid bonds immersed in a homogeneous fluid of viscosity $\eta(T)$. The roto-translational and internal friction and diffusion tensors are calculated as functions of the translational friction of a single free sphere, which at temperature T is obtained simply as $\xi(T) = CR\eta(T)\pi$, which depends on the boundary constant coefficient C and the effective atomic radius R. Calculation of τ_I is relatively straightforward, and it can be further simplified if additional approximations are introduced. In Table 2, we report values for τ_I and the physical characteristic of the different solvents; namely, *n*-hexane, cyclohexane, benzene, dibutyl ether, diethyl ether, *n*-butylchloride, acetonitrile, and dimethylsulfoxide.

Determination of molecular parameters $E_n(\varphi)$, $\boldsymbol{\mu}_n(\varphi)$, τ_I, and τ_S is therefore possible although subject to severe approximation. In principle, kinetic coefficients $k^{nr}_{A\to g}$, $k^{nr}_{B\to g}$, $k^{nr}_{A\to B}$, $k^{nr}_{B\to A}$, $k^{rad}_{A\to g}$, $k^{rad}_{B\to g}$, source function $S_n(\varphi, x)$, and intrinsic line shape $g_n(\omega)$ could be determined independently from quantum mechanical calculations. Here, we shall choose a phenomenological approach, trying to model, in terms of a reduced number of free parameters, most of the expected features of these quantities.[31] To this purpose, we start by assuming simple functional forms for the kinetic coefficients, chosen to summarize known emission properties of DMABN: (i) $k^{nr}_{A\to B}$, $k^{nr}_{B\to g}$, and $k^{rad}_{B\to g}$ are assumed to be monotonically increasing with increasing φ and to have a maximum at $\varphi \approx \pi/2$; (ii) $k^{nr}_{B\to A}$, $k^{nr}_{A\to g}$, and $k^{rad}_{A\to g}$ are assumed to have a maximum at $\varphi \approx 0$ and to be monotonically decreasing with increasing φ; (iii) only two effective solvent- and temperature-independent parameters, k^{nr} and k^{rad}, are introduced to measure radiative and nonradiative emission strength, and a simple squared cosine/sine dependence upon φ is allowed. It follows that $k^{nr}_{A\to g} \approx k^{nr}\cos^2\varphi$, $k^{nr}_{B\to g} \approx k^{nr}\sin^2\varphi$, $k^{nr}_{A\to B} \approx k^{nr}\sin^2\varphi$, $k^{nr}_{B\to A} \approx k^{nr}\cos^2\varphi$, $k^{rad}_{A\to g} \approx k^{rad}\cos^2\varphi$, and $k^{rad}_{B\to g} \approx k^{rad}\sin^2\varphi$. The matrix of coefficients $\mathbf{k} = \{k_{n,n'}\}$ in eq 3 takes the form

$$\mathbf{k} = \begin{pmatrix} k^{nr}\sin^2\varphi + k\cos^2\varphi & -k^{nr}\cos^2\varphi \\ -k^{nr}\sin^2\varphi & k^{nr}\cos^2\varphi + k\sin^2\varphi \end{pmatrix} \quad (10)$$

where $k = k^{nr} + k^{rad}$. It should be noted that the given expression for matrix $\mathbf{k}$ is purely phenomenological, and it can be considered simply a convenient interpolative approximation for known qualitative features of radiative and nonradiative constants.[56]

The intrinsic line shape $g_n(\omega)$ is simply estimated as a Gaussian function with constant linewidth L, $g_n(\omega) \approx g(\omega) =$

$\exp(-\omega^2/2L^2)/(2\pi L^2)^{1/2}$, and we postpone the definition of source function $S_n(\varphi, x)$ to section III for convenience of notation.

III. DMABN: Model Treatment

A. Approximate Emission Fluorescence. We shall start by introducing a reduced solvent variable $\tilde{x} = x/(F_{or}k_BT)^{1/2}$. The energy function for state n becomes

$$\frac{E_n}{k_BT} = \frac{\epsilon_n - F_0\mu_n{}^2/2}{k_BT} + \frac{1}{2}(\tilde{x}-\tilde{x}_n)^2 = \tilde{V}_n(\varphi) + \frac{1}{2}(\tilde{x}-\tilde{x}_n)^2 \tag{11}$$

where $\tilde{x}_n = (F_{or}/k_BT)^{1/2}\mu_n$. The emission fluorescence is given explicitly by eq 3—where we remind now that $Q = (\varphi, \tilde{x})$—provided that numerical or analytical solution are obtained for the stationary populations $P_{st,n}$, which is obtained by solving eq 3 which takes the explicit form

$$-\left(\frac{1}{\tau_I}\frac{\partial}{\partial\varphi}P_{eq,n}\frac{\partial}{\partial\varphi}P_{eq,n}{}^{-1} + \frac{1}{\tau_S}\frac{\partial}{\partial\tilde{x}}P_{eq,n}\frac{\partial}{\partial\tilde{x}}P_{eq,n}{}^{-1}\right)P_{st,n} + \sum_{n'}k_{nn'}P_{st,n'} = S_n \tag{12}$$

Instead of resorting to an exact solution, we introduce the approximate *ansatz* $P_{st,n} \approx p_{st,n}G(\tilde{x} - \tilde{x}_{st,n})$, where $p_{st,n}(\varphi)$ and $\tilde{x}_{st,n}(\varphi)$ are functions, to be determined, of the torsional angle only and $G(\tilde{x}) = \exp(-\tilde{x}^2/2)/(2\pi)^{1/2}$, i.e., a Gaussian function of width equal to 1. Notice that $P_{eq,n} = p_nG(\tilde{x} - \tilde{x}_n)$, where p_n is the Boltzmann distribution over $\tilde{V}_n$.

The approximated emission fluorescence is then given by

$$I(\omega) \propto \sum_n \int d\varphi\, k_n^{rad}(\varphi)\, p_{st,n}(\varphi) \int d\tilde{x} g[\omega - \Delta\omega_n(\varphi,\tilde{x})]\, G[\tilde{x} - \tilde{x}_{st,n}(\varphi)] \tag{13}$$

The integration with respect to the $\tilde{x}$ variable can be carried on analytically, since it is easily reduced to the exponential of second degree polynomial in $\tilde{x}$. The resulting expression is

$$I(\omega) \propto \sum_n \int d\varphi\, k_{n\to g}^{rad}(\varphi)\, p_{st,n}(\varphi)\, i_n(\omega,\varphi)$$
$$i_n(\omega,\varphi) = \exp\left\{-\frac{[\omega - \omega_q(\Delta\tilde{x}_n\Delta\tilde{x}_{st,n} + \Delta\tilde{V}_n)]^2}{2(\omega_q{}^2\Delta\tilde{x}_n{}^2 + L^2)}\right\}\Big/ [2\pi(\omega_q{}^2\Delta\tilde{x}_n{}^2 + L^2)]^{1/2} \tag{14}$$

where $\omega_q = k_BT/\hbar$, $\Delta\tilde{x}_n = \tilde{x}_g - \tilde{x}_n$, $\Delta\tilde{V}_n = \tilde{V}_n - \tilde{V}_g$. Equation 14, combined with the evaluation of $p_{st,n}(\varphi)$ and $\tilde{x}_{st,n}(\varphi)$ is the main result of this work, since it allows a direct link between emission fluorescence signal and model parameters. The signal is in fact given by a convolution, with respect to reduced stationary population $p_{st,n}(\varphi)$ and radiative coefficient $k_n^{rad}(\varphi)$ for each excited state n of Gaussian functions $i_n(\omega, \varphi)$ centered in $\omega_q(\Delta\tilde{x}_n\tilde{x}_{st,n} + \tilde{V}_n)$ and with width $(\omega_q{}^2\Delta\tilde{x}_n{}^2 + L^2)^{1/2}$. Notice that solvent polarity enters mainly by defining the local emission center, for a given value of the torsional angle, in the function $i_n(\omega, \varphi)$, and secondarily by introducing an additional broadening to L of the order of $\omega_q\Delta\tilde{x}_n$.

B. Stationary Populations. The functions $p_{st,n}(\varphi)$ and $\tilde{x}_{st,n}(\varphi)$ can be obtained by substituting the chosen *ansatz* form for $P_{st,n}$ in eq 4. We have yet to define the source function. A reasonable assumption is that only direct excitation of the B state is allowed,[45,51] and thus, a simple choice is $S_n = \omega_S\delta_{n,B}P_{eq,B} = \omega_S\delta_{n,B}p_BG(\tilde{x} - \tilde{x}_B)$, where ω_S is an arbitrary constant with the dimension of a frequency.

Closed expressions for $p_{st,n}(\varphi)$ and $\tilde{x}_{st,n}(\varphi)$ can now be obtained from eq 12 via a simple moment expansion. If an average of eq 12 with respect to $\tilde{x}$ is taken, the following equation is obtained

$$-\frac{1}{\tau_I}\frac{\partial}{\partial\varphi}\left[p_n\frac{\partial}{\partial\varphi}p_n{}^{-1} - (\tilde{x}_{st,n} - \tilde{x}_n)\frac{d\tilde{x}_n}{d\varphi}\right]p_{st,n} + \sum_{n'}k_{nn'}p_{st,n'} = \omega_S\delta_{n,B}p_B \tag{15}$$

By multiplying eq 12 by $\tilde{x}$ and then integrating in $\tilde{x}$, one gets

$$-\frac{1}{\tau_I}\frac{\partial}{\partial\varphi}\left\{p_n\frac{\partial}{\partial\varphi}p_n{}^{-1}\tilde{x}_{st,n} + [\tilde{x}_{st,n}(\tilde{x}_{st,n} - \tilde{x}_n) - 1]\frac{d\tilde{x}_n}{d\varphi}\right\}p_{st,n} + \frac{1}{\tau_S}(\tilde{x}_{st,n} - \tilde{x}_n)p_{st,n} + \sum_{n'}k_{nn'}p_{st,n'}\tilde{x}_{st,n'} = \omega_S\delta_{n,B}p_n\tilde{x}_n \tag{16}$$

Since $\tau_S \ll \tau_I$ (cfr. section III.C), a simplified expression is obtained by neglecting the first term in the rhs of eq 16. Notice that, since the emission signal is determined minus an arbitrary constant factor, we can choose conveniently to set $p_{st,n} \to \tau_I\omega_S p_{st,n}$. Equations 15 and 16 can then be written in their final form

$$-\frac{\partial}{\partial\varphi}\left[p_n\frac{\partial}{\partial\varphi}p_n{}^{-1} - (\tilde{x}_{st,n} - \tilde{x}_n)\frac{d\tilde{x}_n}{d\varphi}\right]p_{st,n} + \sum_{n'}c_{nn'}p_{st,n'} = \delta_{n,B}p_B$$
$$\rho(\tilde{x}_{st,n} - \tilde{x}_n)p_{st,n} + \sum_{n'}c_{nn'}p_{st,n'}\tilde{x}_{st,n'} = \delta_{n,B}p_B\tilde{x}_B \tag{17}$$

where $c_{nn'} = \tau_Ik_{nn'}$, $\rho = \tau_I/\tau_S$. Under the additional hypothesis that $\rho \gg c_{nn'}$ (i.e., $\tau_S \ll k^{nr}, k^{rad}$ meaning that solvent relaxation is considered fast also with respect to radiative and nonradiative emission coefficients), the approximate solution $\tilde{x}_{st,A} \approx \tilde{x}_A$ and $\tilde{x}_{st,B} \approx \{1 + [1 + (1/\rho)(p_B/p_{st,B})]\}\tilde{x}_B \approx \tilde{x}_B$, if one neglects entirely the correction term $p_B/\rho p_{st,B}$, so that further simplified expressions for $p_{st,n}(\varphi)$ and $\tilde{x}_{st,n}(\varphi)$ are

$$\tilde{x}_{st,n} = \tilde{x}_n$$
$$-\frac{\partial}{\partial\varphi}p_n\frac{\partial}{\partial\varphi}p_n{}^{-1}p_{st,n} + \sum_{n'}c_{nn'}p_{st,n'} = \delta_{n,B}p_B \tag{18}$$

Equations 14 and 17, or 18, can be solved numerically. A finite difference scheme has been employed, on a regular grid of $2K + 1$ nodes $\varphi_k = \delta\varphi k$, with $k = -K, -K+1, \ldots, K-1, K$. Discretization of eq 18 is straightforward, and a standard linear method can be employed to solve for the resulting linear system in the unknown $p_{st,n,k} = p_{st,n}(\varphi_k)$. In the next section, solvatochromic and temperature dependence effects are calculated for the fluorescence emission bands of DMABN in solvents of increasing polarity.

IV. Results and Discussion

Summarizing, the static properties $\varepsilon_n(\varphi)$ and $\mu_n(\varphi)$ in vacuo are obtained from QM calculations; coarse correction to allow for the solvent polar environment is taken into account at the simplified Onsager level, with the parameters $\varepsilon_{0,\infty}$ (dielectric constants) and V (effective molecular volume); τ_I is estimated from hydrodynamic modeling and is directly linked to solvent viscosity η, τ_S available in the literature; parameters k^{nr}, k^{rad}, and L are assumed to be solvent and temperature independent.

TABLE 2: Physical Characteristics and Solvent-Dependent Parameters for DMABN in *n*-Hexane, Dibutyl Ether, Diethyl Ether, *n*-Butylchloride, Acetonitrile, and Dimethylsulfoxide

solvent	viscosity (Pa s)	ε_0	ε_∞	τ_I (ps)	e_A^{corr}	e_B^{corr}
n-hexane (ref 57)	0.294×10^{-3}	1.89	1.88	20.9	−0.46	0.28
dibutyl ether (ref 57)	0.114×10^{-3}	3.10	1.96	8.11	−0.46	0.28
diethyl ether (ref 57)	0.224×10^{-3}	4.20	1.82	16.0	−0.28	0.28
n-butylchloride (ref 58)	0.469×10^{-3}	9.60	1.97	33.4	0	0.28
acetonitrile	0.340×10^{-3} (ref 58)	35.94 (ref 59)	1.80 (ref 59)	24.2	0	0.2
dimethylsulfoxide	1.99×10^{-3} (ref 58)	46.45 (ref 59)	2.18 (ref 59)	141.8	0	0.13

We consider also two additional solvent-dependent corrective factors, to the PES for the A and B states, $e_{A,B}^{corr}$. These are introduced to adjust absolute positions of the calculated spectra with respect to experimental ones, and they can be justified given the very simplified strategy adopted for estimating solvation energy corrections. We can now distinguish between a solvent-independent parameter set and a solvent-dependent parameter set. In the former set, we number the effective molecular volume V, the average atomic radius R, and the boundary constant C for evaluation of τ_I, the amplitude of the elementary Gaussian band L and the cumulative nonradiative and radiative parameters k^{nr}, k^{rad}. The molecular volume is taken equal to $V = 1.2 \times 10^{-28}$ m^3, while the effective radius for the calculation is chosen equal to $R = 1.95$ Å and the constant C has been taken equal to 6, corresponding to stick boundary conditions. The amplitude L has been chosen as $L = 60$ nm. Finally, k^{rad} is set to 15 ps, while k^{nr} is taken equal to 1 ps. Parameters dependent from the solvent are summarized in Table 2, including the correction energies $e_{A,B}^{corr}$. The values obtained for τ_I can be compared with known magnitudes of solvent relaxation times:[57–59] for instance, for benzene (low polarity) and acetonitrile (high polarity), we have $\tau_I = 42.7$ ps, $\tau_S = 2.2$ ps and $\tau_I = 24.2$ ps, $\tau_S = 0.26$ ps, respectively, thus allowing a full justification of the time scale separation invoked previously to simplify the dynamic equations. Correction energies $e_{A,B}^{corr}$ are essentially partitioned in two sets: low and intermediate polarity solvents, for which $e_A^{corr} = -0.46$ eV and $e_B^{corr} = 0.28$ eV, and high-polarity solvents for which the correction energies are smaller in magnitude. This suggests that the rough estimate employed here for solvation energy based on Onsager theory is working, not unsurprisingly, only for highly polar environments, whereas it is a mediocre choice for low-polarity media. The overall comparison of experimental and simulated data is shown in Figure 4, which displays solvatochromic effects calculated for the normalized fluorescence emission of DMABN at room temperature in the eight selected solvents of increasing polarity, namely, *n*-hexane, dibutyl ether, diethyl ether, *n*-butylchloride, acetonitrile, and dimethylsulfoxide. The comparison shows that the model proposed is able to reproduce reasonably well the spectral position and shape of the emission spectra of DMABN, as can also be seen quantitatively from Table 3. In particular, the model reproduces the red shift expected for TICT excited states when the dielectric constant of the solvent increases. The combination of stochastic methods and QM calculation of PES/charge distributions for describing the static and dynamic properties of relatively complex molecules in polar solvents, like the one considered in this report, is potentially useful, based on a combination of continuum treatment (the solvent which is considered a continuous dielectric and/or hydrodynamic fluid) and detailed solute dynamics, but significantly increasing the accuracy employed with respect to previous treatments[15] to define both geometric and dissipative parameters. However, before a real predictive value can be assured for the model in dealing with more complex systems, several improvements and integrations are needed. In the present approach, solvation coordinates are treated in a rather coarse way, and interaction with the solute is considered only via a simplified dipole−solvation polarization term; QM calculations are hardly refined, and in particular, a limited description of internal degrees of freedom is assumed.

TABLE 3: Experimental and Simulated Fluorescence Maxima for LE and TICT Bands in Different Solvents

solvent	LE^{exp} (nm)	$TICT^{exp}$ (nm)	LE^{sim} (nm)	$TICT^{sim}$ (nm)
n-hexane	338 (ref 5)		335	
dibutyl ether	348 (ref 5)		351	
diethyl ether	351 (ref 5)		350	
n-butylchloride	353 (ref 5)	408 (ref 5)	342	400
acetonitrile	361 (ref 60)	471 (ref 60)	352	475
dimethylsulfoxide	358 (ref 61)	479 (ref 61)	348	481

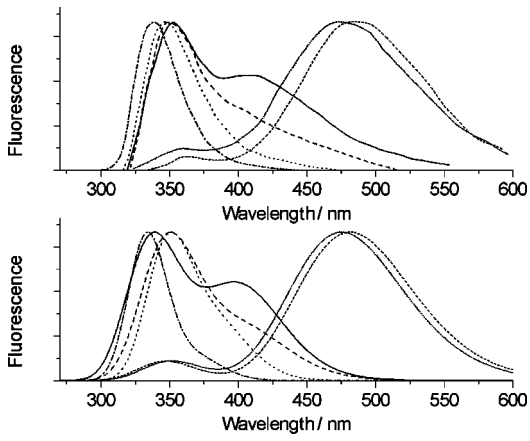

Figure 4. Calculated solvatochromic effects on the static emission of DMABN at $T = 298.15$ K in the solvent series *n*-hexane (dash-dot), dibutyl ether (dot), diethyl ether (dash), *n*-butylchloride (solid), acetonitrile (short dot), and dimethylsulfoxide (short dash). In the top, we report the experimental spectra, while in the bottom, the simulated spectra.

Our main objective in this work has been to discuss the degree of advancement of the integrated computational approach to the interpretation of fluorescence emission of a prototype dual fluorescence probe in solvated environments, via combination of advanced quantum mechanical approaches and stochastic modeling of relaxation processes. Specific stochastic variables can be employed for describing the instantaneous configuration of the local solvent structure, and numerical solutions in semianalytic form can be obtained in terms of correlation functions which are directly linked to the fluorescence signal. Further integration of these building blocks can be used to define a robust and reliable computational approach for ab initio prediction of emission spectroscopic properties of organic molecules in solution. In a companion work,[62] we apply the present stochastic approach to the interpretation of the emission fluorescence of benzonitrile (DMABN−crown5).[21] The covalent attachment of benzonitrile to the nitrogen of a metal binding ionophore creates a fluorescent species that combines the

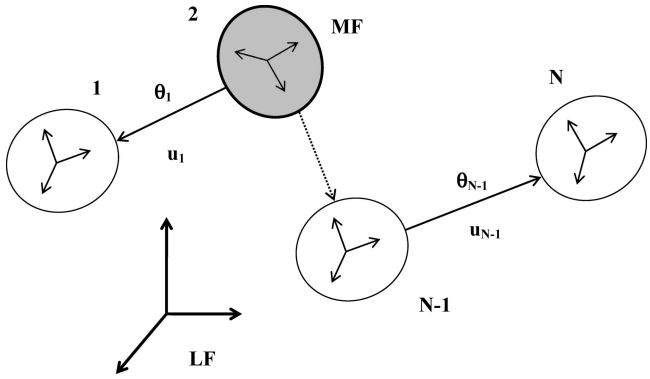

Figure 5. Scheme for the evaluation of the diffusion tensor of a flexible *N*-fragment system; the molecular frame (MF) is fixed on the second fragment.

properties of DMABN with the metal binding properties of the cyclic ether. Emission fluorescence is then calculated by solving the diffusion/sink/source equation for the stationary population of excited states, suitably modified, and compared to experimentally measured emission fluorescence of DMABN−crown5. It is therefore shown that it is possible to model, at a modest computational cost, the dependence of the fluorescence emission of DMABN derivatives on solvation effects, internal flexibility, and molecular geometry, which is a necessary step in the comprehension of complex fluoro-ionophores.

Appendix: Hydrodynamic Evaluation of Diffusion Parameters

Several authors have described the principles and applications of hydrodynamic approaches, The molecule is usually partitioned into a collection of beads, which are chosen to describe the overall shape of the molecule as closely as possible. In the classical bead approximation, each atom or group of atoms is represented by a single bead; the rotational diffusion tensor is obtained by classic arguments.[63,64] An implementation of these principles is provided in the HYDRONMR code[64] which is obtained for rigid molecular systems. However, we need a systematic application of a standard hydrodynamic model to direct evaluation of diffusion (friction) tensorial properties, applicable to flexible molecules for which the internal degrees of freedom are represented by torsional angles.[55] We start from a simplified view of the molecule under investigation as an ensemble of N fragments, each formed by spheres representing atoms or groups of atoms, immersed in a homogeneous isotropic fluid of known viscosity. We assume that the ith fragment is composed by N_i spheres (extended atoms) and that the torsional angle φ_i defines the relative orientation of fragments i and $i + 1$. We denote by $\mathbf{u}_i$ the unitary vector for the corresponding bond. A total of $N - 1$ torsional angles/bonds are present—only noncyclic and nonbranched geometries are considered here—and each fragment has n_i atoms. For convenience, each $\mathbf{u}_i$ points from an atom in fragment i to an atom in fragment $i + 1$ for $i \geq \nu$ and p points from an atom in fragment $i + 1$ to an atom in fragment i for $i < \nu$. Notice that the definition of the MF in a flexible system is somewhat arbitrary, and can be essentially left to convenience arguments. For the sake of simplicity, we may assume that the MF is fixed on generic fragment ν (Figure 5). By definition, *in the MF*, atoms of fragment ν have only translational and rotational motions, while atoms of all other fragments have additional internal rotational motions. Let us now associate the set of coordinates $(\mathbf{R},\Omega,\varphi)$, which describe the translational, rotational, and internal torsional motions, respectively, with the velocities $(\mathbf{V},\omega,\dot{\varphi})$ representing the molecule translational velocity, angular velocity around an inertial frame, and associated torsional momenta. In the presence of constraints in and among fragments, the generalized force, made of force $\mathbf{F}$, torque $\mathbf{N}$, and the internal torques $\mathbf{N}^{\text{int}}$, is related to the generalized velocity by the relation

$$\mathscr{F} = -\Xi\mathscr{V}$$
$$\mathscr{F} = \begin{pmatrix} \mathbf{F} \\ \mathbf{N} \\ \mathbf{N}^{\text{int}} \end{pmatrix}, \qquad \mathscr{V} = \begin{pmatrix} \mathbf{V} \\ \omega \\ \dot{\varphi} \end{pmatrix} \tag{A1}$$

p-formula> while in the absence of constraints a similar relation holds for each single extended atom between its velocity and the force acting on it, which in compact matrix form can be written

$$\mathscr{f} = -\xi\mathscr{v}$$
$$\mathscr{f} = \begin{pmatrix} \mathbf{f}_1^1 \\ \dots \\ \mathbf{f}_{n_N}^N \end{pmatrix}, \qquad \mathscr{v} = \begin{pmatrix} \mathbf{v}_1^1 \\ \dots \\ \mathbf{v}_{n_N}^N \end{pmatrix} \tag{A2}$$

where $\mathbf{f}_j^i$ is the force acting on the jth atom of the ith fragment ($1 \leq j \leq n_i$), etc. Constrained and unconstrained forces and velocities can be related via geometric considerations by the relations $\mathscr{F} = \mathbf{A}\mathscr{f}$ and $\mathscr{v} = \mathbf{B}\mathscr{V}$, where $\mathbf{A}$ and $\mathbf{B}$ are matrices depending on the molecular geometry and one can show easily by inspection that $\mathbf{A} = \mathbf{B}^{\text{tr}}$. It follows that $\Xi = \mathbf{B}^{\text{tr}}\xi\mathbf{B}$. For a system of linearly connected fragments, it is relatively simple to evaluate matrix $\mathbf{B}$. Let $\mathbf{r}_j^i$ be the vector of the jth atom of the ith fragment in the MF. Thus, for atoms belonging to the fragment ν, velocities are $\mathbf{v}_j^\nu = \mathbf{V} + \omega \times \mathbf{r}_j^\nu$, while, for all other atoms, velocities are$\mathbf{v}_j^i = \mathbf{V} + \omega \times \mathbf{r}_j^i + \sum_k \dot{\varphi}_k\mathbf{u}_k \times \mathbf{r}j,k^i\mathbf{v}_j^i = {}^T\mathbf{B}_j^i\mathbf{v} + {}^R\mathbf{B}_j^i\omega + \sum_k {}^I\mathbf{B}j,k^i\dot{\varphi}_k$, where $\mathbf{r}j,k^i$ is the difference between the vector of the jth atom and the atom at the origin of the unit vector $\mathbf{u}_k$ and the sum is taken over fragments that link the reference fragment ν to the fragment i; ${}^T\mathbf{B}_j^i = \mathbf{1}_3$, ${}^R\mathbf{B}_j^i = -r_j^{i\times}$, ${}^I\mathbf{B}_j^i = -\mathbf{r}j,k^i\mathbf{u}_k$ or 0; and finally for vector $\mathbf{a}$, 3×3 matrix $\mathbf{a}^\times$ is defined such that, for a generic vector $\mathbf{b}$, the relation $\mathbf{a} \times \mathbf{b} = \mathbf{a}^\times\mathbf{b}$ holds. By assuming a form for the friction tensor of nonconstrained atoms, ξ, one can calculate the friction for the constrained atoms, Ξ. We assume for simplicity the simplest model for a noninteracting sphere in a fluid, namely, that matrix ξ has only diagonal blocks of the form $\xi(T)\mathbf{1}_3$ where $\xi(T)$ is the translational friction of a sphere of radius R at temperature T and given by the Stokes law $\xi(T) = CR\eta(T)\pi$, where $\eta(T)$ is the solvent viscosity at the given temperature T and C depends on hydrodynamic boundary conditions. The friction is then given as $\Xi = \xi(T)\mathbf{B}^{\text{tr}}\mathbf{B}$. The diffusion tensor (which can be partitioned in translation, rotational, internal, and mixed blocks) can now be obtained as the inverse of the friction tensor.

Acknowledgment. The authors thank the Italian Ministry for Universities and Scientific and Technological Research, grants PRIN ex-40% 2004 and FIRB and the National Institute for Materials Science and Technology, grants PRISMA 2005 and PROMO 2006.

References and Notes

(1) Lippert, E.; Lüder, W.; Moll, F.; Nagele, H.; Boos, H.; Prigge, H.; Siebold-Blankenstein, I. *Angew. Chem.* **1961**, *73*, 695.
(2) Van Der Auweraer, M.; Vannerem, A.; De Schryver, F. C. *J. Mol. Struct.* **1982**, *84*, 343.
(3) Sobolewski, A. L.; Domcke, W. *Chem. Phys. Lett.* **1996**, *250*, 428.
(4) Kim, H. J.; Hynes, J. T. *J. Photochem. Photobiol., A* **1997**, *105*, 337.

(5) Grabowski, Z. R.; Rotkiewicz, K.; Rettig, W. *Chem. Rev.* **2003**, *103*, 3899.
(6) Schamschule, R.; Parusel, A. B. J.; Khler, G. *THEOCHEM* **1997**, *419*, 161.
(7) Mennucci, B.; Toniolo, A.; Tomasi, J. *J. Am. Chem. Soc.* **2000**, *122*, 10621.
(8) Suldholt, W.; Sobolewski, A. L.; Domcke, W. *Chem. Phys.* **1999**, *204*, 9.
(9) Nordio, P. L.; Polimeno, A.; Barbon, A. *Pol. J. Chem.* **1993**, *67*, 1397.
(10) Grabowski, Z. R. *Pure Appl. Chem.* **1992**, *64*, 1249.
(11) Nordio, P. L.; Polimeno, A. *Mol. Phys.* **1992**, *75*, 1203.
(12) Polimeno, A.; Saielli, G.; Nordio, P. L. *Chem. Phys.* **1998**, *235*, 313.
(13) Moro, G. J.; Nordio, P. L.; Polimeno, A. *Mol. Phys.* **1989**, *68*, 1131.
(14) Giacometti, G.; Moro, J. G.; Nordio, P. L.; Polimeno, A. J. *Mol. Liq.* **1989**, *42*, 19.
(15) Polimeno, A.; Barbon, A.; Nordio, P. L.; Rettig, W. *J. Phys. Chem.* **1994**, *98*, 12158.
(16) Van Der Auweraer, M.; Grabowski, Z. R.; Rettig, W. *J. Phys. Chem.* **1991**, *95*, 2083.
(17) Von Der Haar, T.; Hebecker, A.; Il'chev, Y.; Jiang, Y. B.; Khne, W.; Zachariasse, K. A. *Recl. Trav. Chim. Pays-Bas* **1995**, *114*, 430.
(18) Collins, G. E.; Choi, L. S.; Callahan, J. H. *J. Am. Chem. Soc.* **1998**, *120*, 1474.
(19) Choi, L. S.; Collins, G. E. *Chem. Commun.* **1998**, 893.
(20) de Lange, M. M. C.; Leeson, D. T.; Van Kuijk, K. A. B.; Huizer, A. H.; Varma, C. A. G. O. *Chem. Phys.* **1993**, *177*, 43.
(21) Letard, J. F.; Delmond, S.; Lapouyade, R.; Braun, D.; Rettig, W.; Kreissler, M. *Recl. Trav. Chim. Pays-Bas* **1995**, *14*, 517.
(22) Zare, R. N. *Angular Momentum: Understanding Spatial Aspects in Chemistry and Physics*; John Wiley & Sons: New York, 1988.
(23) Parr, R. G.; Yang, W. *Density-Functional Theory of Atoms and Molecules*; Oxford University Press: Oxford, U.K., 1989.
(24) Quinones, E.; Ishikawa, Y.; Leszczynski, J. *THEOCHEM* **2000**, *529*, 127.
(25) Purkayastha, P.; Bhattacharyya, P. K.; Bera, S. C.; Chattopadhyay, N. *Phys. Chem. Chem. Phys.* **1999**, *105*, 4182.
(26) Tomin, V. I.; Brozis, M. *Opt. Spectrosc.* **2005**, *100*, 546.
(27) Parusel, A. B. J.; Rettig, W.; Sudholt, W. J. *J. Phys. Chem. A* **2002**, *106*, 804.
(28) Lommatzsch, U.; Brutschy, B. *Chem. Phys.* **1998**, *234*, 35.
(29) Foreman, J. B.; Head-Gordon, M.; Pople, J. A.; Frisch, M. J. *J. Phys. Chem.* **1992**, *96*, 135.
(30) Cogan, S.; Zilberg, S.; Haas, Y. *J. Am. Chem. Soc.* **2006**, *128*, 3335.
(31) Xu, X.; Cao, Z.; Zhang, Q. *J. Chem. Phys.* **2005**, *122*, 194395.
(32) Chiba, M.; Tsuneda, T.; Hirao, K. *J. Chem. Phys.* **2007**, *126*, 034504.
(33) Rappoport, D.; Furche, F. *J. Am. Chem. Soc.* **2004**, *126*, 1277.
(34) Parusel, A. B. J. *Phys. Chem. Chem. Phys.* **2000**, *2*, 5545.
(35) Scalmani, G.; Frisch, M. J.; Mennucci, B.; Tomasi, J.; Cammi, R.; Barone, V. *J. Chem. Phys.* **2006**, *124*, 094107/1.
(36) Wanko, M.; Garavelli, M.; Bernardi, F.; Niehaus, T. A.; Frauenheim, T.; Elstner, M. *J. Chem. Phys.* **2004**, *120*, 1674.
(37) Tozer, D. J.; Amos, R. D.; Handy, N. C.; Roos, B. O.; Serrano-Andres, L. *Mol. Phys.* **1999**, *97*, 859.
(38) Dreuw, A.; Weisman, J. L.; Head-Gordon, M. *J. Chem. Phys.* **2003**, *119*, 2943.
(39) Dreuw, A.; Head-Gordon, M. *J. Am. Chem. Soc.* **2004**, *126*, 4007.
(40) Burke, K.; Werschnik, J.; Gross, E. K. U. *J. Chem. Phys.* **2005**, *123*, 62206.
(41) Gritsenko, O.; Baerends, E. J. *J. Chem. Phys.* **2004**, *121*, 655.
(42) Tawada, Y.; Tsuneda, T.; Yanagisawa, S.; Yanai, T.; Hirao, K. *J. Chem. Phys.* **2004**, *120*, 8425.
(43) Maitra, N. T.; Zhang, F.; Cave, R. J.; Burke, K. *J. Chem. Phys.* **2004**, *120*, 5932.
(44) Maitra, N. T. *J. Chem. Phys.* **2005**, *122*, 234104.
(45) Adamo, C.; Barone, V. *J. Chem. Phys.* **1999**, *110*, 6158.
(46) Adamo, C.; Scuseria, G. E.; Barone, V. *J. Chem. Phys.* **2000**, *111*, 2889.
(47) Improta, R.; Barone, V. *J. Am. Chem. Soc.* **2004**, *126*, 14320.
(48) Frisch, M. J.; Pople, J. A.; Binkley, J. S. *J. Chem. Phys.* **1984**, *80*, 3265.
(49) Dunning, T. H., Jr *J. Chem. Phys.* **1989**, *90*, 1007.
(50) Petersson, G. A.; Al-Laham, M. A. *J. Chem. Phys.* **1991**, *94*, 6081.
(51) Bulliard, C.; Allan, M.; Wirtz, G.; Haselbach, E.; Zachariasse, K. A. *J. Phys. Chem. A* **1999**, *103*, 7766.
(52) Serrano-Andrés, L.; Merchán, M.; Roos, B. O.; Lindh, R. *J. Am. Chem. Soc.* **1995**, *117*, 3198.
(53) Parusel, A. B. J.; Köhler, G.; Nooijen, M. *J. Phys. Chem. A* **1999**, *103*, 4056.
(54) Frisch, M. J.; et al. *Gaussian 03*, revision C.02; Gaussian, Inc.: Pittsburgh, PA, 2003.
(55) Moro, G. *Chem. Phys.* **1987**, *118*, 167.
(56) Lippert, E.; Rettig, W.; Bonačić-Koutecký, V.; Heisel, F.; Miehé, J. A. *Adv. Chem. Phys.* **1987**, *68*, 1.
(57) *Handbook of Chemistry and Physics*, 64th ed.; CRC Press: Boca Raton, FL, 1983.
(58) Horng, M. L.; Gardecki, J. A.; Papazyan, A.; Maroncelli, M. *J. Phys. Chem.* **1995**, *99*, 17311.
(59) Horng, M. L.; Dahl, K.; Jones, G.; Maroncelli, M. *Chem. Phys. Lett.* **1999**, *315*, 363.
(60) Murali, S.; Kharlanov, V.; Rettig, W.; Tolmachev, A. I.; Kropachev, A. V. *J. Phys. Chem. A* **2005**, *109*, 6420.
(61) Haidekker, M. A.; Brady, T. P.; Lichlyter, D.; Theodorakis, E. A. *Bioorg. Chem.* **2005**, *33*, 415.
(62) Carlotto, S.; Benzi, C.; Riccò, R.; Ferrante, C.; Maggini, M.; Polimeno, A.; Barone,V. Submitted to *Chem. Phys. Lett.*
(63) De La Torre, J. G.; Bloomfield, V. A. Q. *Rev. Biophys.* **1981**, *14*, 81.
(64) De La Torre, J. G.; Huertas, M. L.; Carrasco, B. *J. Magn. Reson., Ser. B* **2000**, *147*, 138.

JP076676Z